Effective drift and diffusivity in non-Gaussian random gradient flows

I T Drummond, R R Horgan and C A da Silva Santos

Department of Applied Mathematics and Theoretical Physics, University of Cambridge, Silver Street, Cambridge CB3 9EW, UK

Abstract. We study the long-range effective drift and diffusivity of a particle in a random medium moving subject to a given molecular diffusivity and a local drift. The local drift models the effect of a random electrostatic field on a neutral but polarizable molecule. Although the electrostatic field is assumed to obey Gaussian statistics the induced statistics of the drift velocity field are non-Gaussian.

We show that a four-loop perturbation theory calculation of the effective diffusivity is in rather good agreement with the outcome of a numerical simulation for a reasonable range of the disorder parameter. We also measure the effective drift in our simulation and confirm the validity of the 'Einstein relation' that expresses the equality of the renormalization factors, induced by the random medium, for the effective drift and effective diffusivity, relative to their molecular values. The Einstein relation has previously only been confirmed for Gaussian random drift fields. The simulation result, for our non-Gaussian drift model, is consistent with a previous theoretical analysis showing the Einstein relation should remain true, independently of the precise character of the statistics of the drift velocity field.

1. Introduction

The advective diffusion of passive scalar fields in random environments has been extensively studied by both analytical and numerical techniques, with particular emphasis on the computation of effective parameters for a diffusion process that combines molecular diffusion with a drift term that depends linearly on the gradient of a random scalar field [1–10].

The problem is well studied and understood in the case of transport by a gradient velocity field which exhibits *Gaussian* statistics. In isotropic systems a renormalization group approach can be shown to give exact results in one and two dimensions [1–3]. Somewhat surprisingly the same approach works extremely well for the isotropic problem in three dimensions [4–7], though the situation is less clear in the absence of isotropy [8, 9].

One ingredient in the success of the renormalization group method is that, at each stage of the calculation, it respects the Einstein relation that guarantees the equality of the renormalization factors of the effective diffusivity, κ_e, and drift, λ_e, parameters relative to their molecular values, κ_0 and λ_0 respectively. That is

$$\frac{\kappa_e}{\kappa_0} = \frac{\lambda_e}{\lambda_0}. \tag{1}$$

This result does not hold in the, somewhat arbitrary, Hartree–Fock resummation procedure which turns out to be even less accurate than simple low-order perturbation theory which also breaks down for strong disorder.

It turns out that the Einstein relation holds in a wide range of circumstances including ones where the diffusivity and drift coefficient have non-trivial tensorial structure [10]. The only requirement is that the two tensors are linearly dependent. Thus if at the molecular level we have $\lambda_{0\,ij} = \tau\kappa_{0\,ij}$ then we will find for the macroscopic effective parameters that $\lambda_{e\,ij} = \tau\kappa_{e\,ij}$. The isotropic situation is an example of this. The reason that the proportionality factor survives renormalization can be traced back to the existence of a finite sample equilibrium distribution with a vanishing microcurrent. In equilibrium statistical mechanics this vanishing is guaranteed which explains the emergence of the Einstein relation in this context. In the quenched models with which we are concerned the Einstein relation is not guaranteed except in the special but important circumstances indicated above. Given these conditions of proportionality of the molecular tensors however, the Einstein relation can be shown to hold sample by sample. It follows that the relation will hold *independent* of the precise nature of the statistics of the gradient velocity field. This theoretical prediction [10] lends considerable interest to the results of the numerical simulation of the physically motivated model that we study in this paper, in which the gradient velocity field does not have Gaussian statistics.

A physical realization of the *Gaussian* case is the diffusion of an ion in a sea of fixed, disordered charges that give rise to an electrostatic potential. Such a situation can be created by embedding fixed ions in the rather accommodating structure of a zeolite matrix. It is not unreasonable to treat the resulting electrostatic field as having Gaussian statistics at lengthscales somewhat larger than the molecular level but very short compared with macroscopic scales. A related problem, particularly relevant to applications in chemical processes, concerns the diffusion of a *neutral* molecule in such a medium. The case of the diffusion of benzene in zeolites with random ionic inclusions has been studied experimentally and has important technological applications [11]. In this situation the force on the molecule arises because of the interaction of its induced dipole moment with the electrostatic field produced by the included ions. The result is a gradient velocity field with *non*-Gaussian statistics. For simplicity we take it for granted that all tensorial effects are absent.

We assume that the dipole moment P_i of the diffusing particle is proportional to the ambient electric field E_i thus

$$P_i = \mu E_i. \tag{2}$$

The force on the molecule is

$$F_i = P_j \partial_j E_i \tag{3}$$

and since for an electrostatic field $\partial_j E_i = \partial_i E_j$, it follows that

$$F_i = \mu E_j \partial_i E_j = \tfrac{1}{2}\mu \partial_i E_j^2. \tag{4}$$

If we introduce the electrostatic potential $\phi(x)$ then the force on the molecule becomes

$$F_i = \tfrac{1}{2}\mu \partial_i (\nabla\phi(x))^2. \tag{5}$$

If we assume that the drift of the molecule is given by

$$u_i(x) = \nu F_i \tag{6}$$

then, absorbing all constants into an overall parameter λ_0, we have

$$u_i(x) = \tfrac{1}{2}\lambda_0 \partial_i (\nabla\phi(x))^2. \tag{7}$$

It is still reasonable to model the statistical properties of the electrostatic potential $\phi(x)$ by a Gaussian field. However, because of the quadratic relationship between $u_i(x)$ and $\phi(x)$ the statistics of the drift velocity are *not* Gaussian in this model. The higher cumulants of

the velocity field beyond the second do not vanish. Indeed it is very clear that the third- and other odd-order cumulants exist. This means that the problem is not symmetrical under the change $\lambda_0 \to -\lambda_0$. For this reason we explore both positive and negative values of λ_0 even though the physical derivation of the model suggests that $\lambda_0 > 0$. For the purposes of the simulation we take the opportunity to absorb the normalization of $\phi(x)$ into the definition of λ_0 and require

$$\langle (\phi(x))^2 \rangle = 1. \tag{8}$$

The problem we address then, is the evaluation of the long-range effective parameters in terms of the (non-Gaussian) statistical properties of the random flow. Such a model presents its own new technical difficulties. Calculational schemes such as self-consistent perturbation theory or the renormalization group (RG), which proved so successful in Gaussian problems, turn out to be hard to apply to this particular problem. The barriers to a straightforward application of these more sophisticated perturbation methods arise mainly because of the increased complexity of the vertex structure at low wavenumber that is quickly revealed by perturbation theory. In addition the lowest-order correction to the propagator begins at two loops rather than one loop as in the Gaussian case. In this paper we confine ourselves to computing the standard perturbation expansion for the effective diffusivity to four-loop order. As will become clear the results are consistent with the outcome of our numerical simulation of the model over a significant range of values for the drift parameter.

2. Perturbation theory

The diffusion equation in which we are interested has the form

$$\frac{\partial P(x,t)}{\partial t} = \nabla \cdot (\kappa_0 \nabla P(x,t) - u(x)P(x,t)). \tag{9}$$

Here, $P(x,t)$ is the probability density of a particle moving according to the equation

$$\dot{x} = u(x) + w(t) \tag{10}$$

where $w(t)$ is a white noise term that satisfies

$$\langle w_i(t) \rangle = 0 \qquad \text{and} \qquad \langle w_i(t)w_j(t') \rangle = 2\kappa_0 \delta_{ij} \delta(t - t'). \tag{11}$$

The flow field, $u(x)$, is taken to be time independent and is the gradient of a scalar field

$$u(x) = \lambda_0 \nabla \psi(x) \tag{12}$$

but, because the flow originates in the interaction of the induced dipole moment of the diffusing particle with the electrostatic field, $\psi(x)$ does not exhibit Gaussian statistics. In fact, as indicated above, we have

$$\psi(x) = \tfrac{1}{2}(\nabla \phi(x))^2 \tag{13}$$

where $\phi(x)$ is a homogeneous Gaussian random field characterized by the disorder averages

$$\langle \phi(x) \rangle = 0 \qquad \text{and} \qquad \langle \phi(x)\phi(y) \rangle = \Delta(x - y). \tag{14}$$

For simplicity we take the disorder to be isotropic, that is, $\Delta = \Delta(|x|)$.

The perturbative approach to solving equation (9) is well known [1–3, 6, 12, 14, 15] and we only summarize here the necessary results. Since we are interested in the effective parameters governing the evolution of the distribution $P(x,t)$, we study the related static Green function, $G(x)$, which satisfies

$$\kappa_0 \nabla^2 G(x) - \nabla \cdot (u(x)G(x)) = -\delta(x). \tag{15}$$
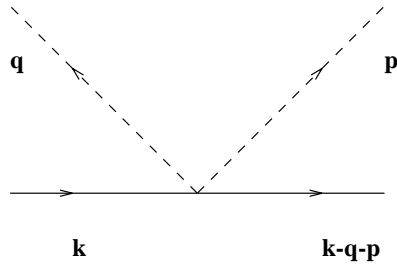
Figure 1. Vertex diagram.

A perturbation series in the coupling λ_0 for $\tilde{G}(\boldsymbol{k})$ can be generated by iterating the formal solution to equation (15) in Fourier space:

$$\tilde{G}(\boldsymbol{k}) = \frac{1}{\kappa_0 k^2} - \frac{\lambda_0}{\kappa_0 k^2} \int \frac{\mathrm{d}^3 q}{(2\pi)^3} \frac{\mathrm{d}^3 p}{(2\pi)^3} \tilde{G}(\boldsymbol{k} - \boldsymbol{q} - \boldsymbol{p})\tilde{\phi}(\boldsymbol{q})\tilde{\phi}(\boldsymbol{p})\frac{\boldsymbol{q}\cdot\boldsymbol{p}\; \boldsymbol{k}\cdot(\boldsymbol{q}+\boldsymbol{p})}{2}. \tag{16}$$

The Green function averaged over the velocity ensemble, $\langle\tilde{G}(\boldsymbol{k})\rangle$, can be written as

$$\langle\tilde{G}(\boldsymbol{k})\rangle = \frac{1}{\kappa_0 k^2 - \sum(\boldsymbol{k})} \tag{17}$$

where the averaging over the velocity ensemble is done using Wick's theorem to give a diagrammatic expansion and $\sum(\boldsymbol{k})$ is the summation of one-particle irreducible diagrams. The expected asymptotic behaviour of the diffusion process at large distances and times implies that the small $\boldsymbol{k}$ behaviour of $\langle\tilde{G}(\boldsymbol{k})\rangle$ is given by

$$\kappa_e = \kappa_0 - \frac{\mathrm{d}}{\mathrm{d}k^2}\sum(\boldsymbol{k})|_{k=0} \tag{18}$$

where κ_e is the effective diffusivity. The Feynman rules for the diagrammatic expansion are as follows:

(1) the wavevector is conserved at each vertex;

(2) each full line carries a factor $1/\kappa_0 k^2$;

(3) the wavevector is integrated around closed loops with a factor $\mathrm{d}^3 q/(2\pi)^3$;

(4) each vertex, whose diagrammatic representation is shown in figure 1, carries a factor $-\lambda_0 \boldsymbol{q}\cdot\boldsymbol{p}\; \boldsymbol{k}\cdot(\boldsymbol{q}+\boldsymbol{p})$;

(5) each internal broken line carries a factor $\tilde{\Delta}(\boldsymbol{q})$;

(6) each diagram must be divided by the usual symmetry factor.

In what follows, we use the explicit spectrum

$$\tilde{\Delta}(\boldsymbol{q}) = \frac{(2\pi)^{3/2}}{k_0^3}\mathrm{e}^{-q^2/2k_0^2}. \tag{19}$$

The normalization is chosen so that $\langle(\phi(\boldsymbol{x}))^2\rangle = 1$. In our numerical calculations, we set $k_0 = 1$.

There is no one-loop correction to the propagator. As mentioned before, this together with the fact that *new* vertices are generated when correcting the primitive one makes it extremely delicate to implement other perturbative schemes such as self-consistent or RG methods. Therefore, we concentrate on a straightfoward perturbation theory calculation which has to be carried out to at least four-loop order to get a sensible outcome. The formal manipulations of which we make use are basically the same as those utilized in [5–7] and we only elucidate the more elaborate steps and state the main results.
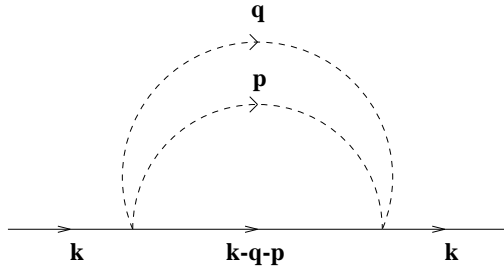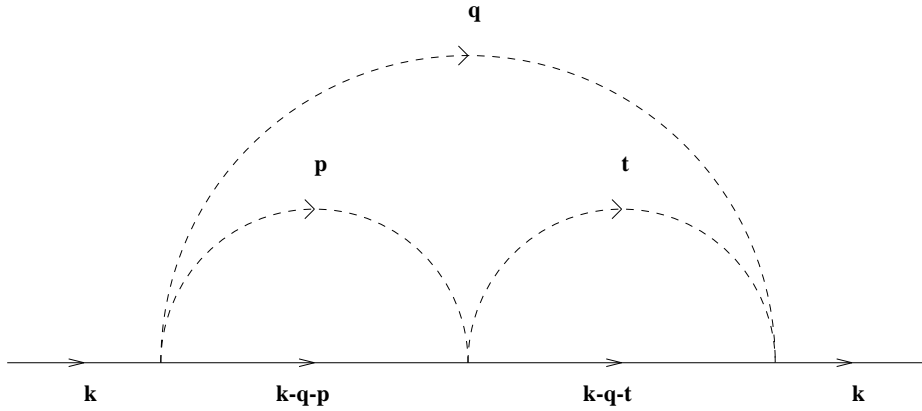
Figure 2. Two-loop contribution to $\sum(k)$.

Figure 3. Three-loop contribution to $\sum(k)$.

The two-loop contribution to $\sum(k)$ is associated with the diagram in figure 2. According to the above Feynman rules it is

$$\overset{(2)}{\sum}(k) = -\frac{1}{2}\frac{\lambda_0^2}{\kappa_0} \int \frac{\mathrm{d}^3q}{(2\pi)^3}\frac{\mathrm{d}^3p}{(2\pi)^3}\tilde{\Delta}(q)\tilde{\Delta}(p)\frac{(p \cdot q)^2 k \cdot (p+q)(k-q-p) \cdot (q+p)}{(k-q-p)^2} \qquad (20)$$

and it can be easily computed to $\mathrm{O}(k^2)$ with the result

$$\overset{(2)}{\sum}(k) = \frac{1}{2}\frac{\lambda_0^2}{\kappa_0}k^2. \qquad (21)$$

In order to encounter deviations from Gaussian behaviour we must calculate beyond second order and consider the three-point correlator of the velocity field, that is, to include the first non-zero odd power in λ_0 in the perturbation expansion. The three-loop diagram contributing to $\sum(k)$ is shown in figure 3 and yields

$$\overset{(3)}{\sum}(k) = -\frac{\lambda_0^3}{\kappa_0^2} \int \frac{\mathrm{d}^3q}{(2\pi)^3}\frac{\mathrm{d}^3p}{(2\pi)^3}\frac{\mathrm{d}^3t}{(2\pi)^3}\tilde{\Delta}(q)\tilde{\Delta}(p)\tilde{\Delta}(t)q{\cdot}p\ p{\cdot}t\ q{\cdot}t$$
$$\frac{k \cdot (q+p)(k-q-p) \cdot (t-p)(k-q-t) \cdot (q+t)}{(k-q-p)^2(k-q-t)^2}. \qquad (22)$$

The numerator can be rewritten using the identity

$$(k-q-t) \cdot (-q-t) = (k-q-t)^2 - k \cdot (k-q-t). \qquad (23)$$

We then have

$$\sum^{(3)}(k) = -\frac{\lambda_0^3}{\kappa_0^2} \int \frac{d^3q}{(2\pi)^3} \frac{d^3p}{(2\pi)^3} \frac{d^3t}{(2\pi)^3} \tilde{\Delta}(q)\tilde{\Delta}(p)\tilde{\Delta}(t) q{\cdot}p \; p{\cdot}t \; q{\cdot}t$$
$$k{\cdot}(q+p)(k-q-p)\cdot(p-t)$$
$$\times \left\{ \frac{1}{(k-q-p)^2} - \frac{k\cdot(k-q-t)}{(k-q-p)^2(k-q-t)^2} \right\}. \tag{24}$$

The first term, which turns out to be the dominant one, can be performed analytically whereas the second one, much smaller, has to be done numerically to $O(k^2)$. It is instructive to explain in some detail how to compute the analytical contribution to $\sum^{(3)}(k)$. In the first term of equation (24), the term odd in t integrates to zero and, moreover, it can be symmetrized for p and q to yield the result

$$\sum^{(3)}_{an}(k) = -\frac{1}{2}\frac{\lambda_0^3}{\kappa_0^2} \int \frac{d^3q}{(2\pi)^3} \frac{d^3p}{(2\pi)^3} \frac{d^3t}{(2\pi)^3} \tilde{\Delta}(q)\tilde{\Delta}(p)\tilde{\Delta}(t) q{\cdot}p \; p{\cdot}t \; q{\cdot}t$$
$$\frac{k\cdot(q+p)(k-q-p)\cdot(q+p)}{(k-q-p)^2}. \tag{25}$$

Using again equation (23) (for vectors p and q) leads to

$$\sum^{(3)}_{an}(k) = \frac{1}{2}\frac{\lambda_0^3}{\kappa_0^2} \int \frac{d^3q}{(2\pi)^3} \frac{d^3p}{(2\pi)^3} \frac{d^3t}{(2\pi)^3} \tilde{\Delta}(q)\tilde{\Delta}(p)\tilde{\Delta}(t) q{\cdot}p \; p{\cdot}t \; q{\cdot}t \; k{\cdot}(q+p)$$
$$\cdot \left\{ 1 - \frac{k\cdot(k-q-p)}{(k-q-p)^2} \right\}. \tag{26}$$

The first term in equation (26) integrates to zero. We need to evaluate the second term only to $O(k^2)$. Because of the explicit factors of k in the integrand we can set $k = 0$ everywhere else to obtain

$$\sum^{(3)}_{an}(k) = \frac{1}{2}\frac{\lambda_0^3}{\kappa_0^2} \int \frac{d^3q}{(2\pi)^3} \frac{d^3p}{(2\pi)^3} \frac{d^3t}{(2\pi)^3} \tilde{\Delta}(q)\tilde{\Delta}(p)\tilde{\Delta}(t) q{\cdot}p \; p{\cdot}t \; q{\cdot}t \frac{k\cdot(q+p)k\cdot(q+p)}{(q+p)^2}. \tag{27}$$

This is easily evaluated as

$$\sum^{(3)}_{an}(k) = \frac{1}{2}\frac{\lambda_0^3}{\kappa_0^2} k^2 \left[\frac{1}{3} \int \frac{d^3q}{(2\pi)^3} q^2 \tilde{\Delta}(q) \right]^3 = \frac{1}{2}\frac{\lambda_0^3}{\kappa_0^2} k^2. \tag{28}$$

Combining the analytical and numerical pieces yields the following result

$$\sum^{(3)}(k) = \frac{\lambda_0^3}{\kappa_0^2} k^2 \left(\frac{1}{2} + 0.030\,375 \right). \tag{29}$$

This last contribution is the first of the odd power terms in the expansions that are responsible for the asymmetry of κ_e under change of sign of the coupling λ_0. Its presence is a direct confirmation of the non-Gaussian property of the statistics of the velocity field. However, truncating the power series at $O(\lambda_0^3)$ causes κ_e to increase for larger negative values of λ_0, as is shown in figure 5. This unphysical feature is obviously an artefact of perturbation theory and can be circumvented by including the fouth-order term in the
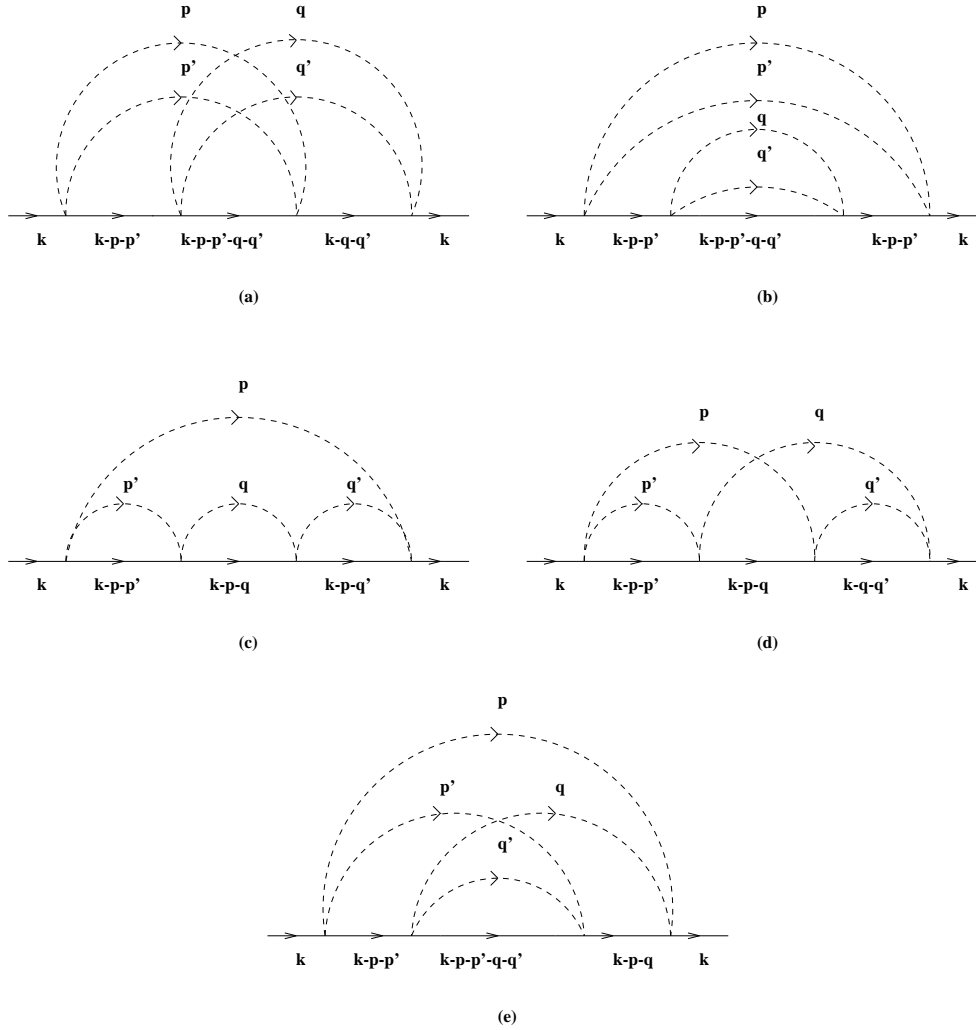
Figure 4. Four-loop contributions to $\sum(\boldsymbol{k})$.

perturbation expansion. The diagrams corresponding to this order are shown in figure 4 and give the following contributions:

$$
\overset{(4a)}{\sum}(\boldsymbol{k}) = \frac{1}{4} \frac{\lambda_0^4}{\kappa_0^3} \int \frac{\mathrm{d}^3 q}{(2\pi)^3} \frac{\mathrm{d}^3 q'}{(2\pi)^3} \frac{\mathrm{d}^3 p}{(2\pi)^3} \frac{\mathrm{d}^3 p'}{(2\pi)^3} \tilde{\Delta}(\boldsymbol{q})\tilde{\Delta}(\boldsymbol{q}')\tilde{\Delta}(\boldsymbol{p})\tilde{\Delta}(\boldsymbol{p}')(\boldsymbol{q}\cdot\boldsymbol{q}')^2(\boldsymbol{p}\cdot\boldsymbol{p}')^2
$$
$$
\boldsymbol{k}\cdot(\boldsymbol{p}+\boldsymbol{p}')(\boldsymbol{k}-\boldsymbol{p}-\boldsymbol{p}')\cdot(\boldsymbol{q}+\boldsymbol{q}')
$$
$$
\frac{(\boldsymbol{k}-\boldsymbol{p}-\boldsymbol{p}'-\boldsymbol{q}-\boldsymbol{q}')\cdot(\boldsymbol{p}+\boldsymbol{p}')(\boldsymbol{k}-\boldsymbol{q}-\boldsymbol{q}')\cdot(\boldsymbol{q}+\boldsymbol{q}')}{(\boldsymbol{k}-\boldsymbol{p}-\boldsymbol{p}')^2(\boldsymbol{k}-\boldsymbol{p}-\boldsymbol{p}'-\boldsymbol{q}-\boldsymbol{q}')^2(\boldsymbol{k}-\boldsymbol{q}-\boldsymbol{q}')^2} \tag{30}
$$
$$
\overset{(4b)}{\sum}(\boldsymbol{k}) = \frac{1}{4} \frac{\lambda_0^4}{\kappa_0^3} \int \frac{\mathrm{d}^3 q}{(2\pi)^3} \frac{\mathrm{d}^3 q'}{(2\pi)^3} \frac{\mathrm{d}^3 p}{(2\pi)^3} \frac{\mathrm{d}^3 p'}{(2\pi)^3} \tilde{\Delta}(\boldsymbol{q})\tilde{\Delta}(\boldsymbol{q}')\tilde{\Delta}(\boldsymbol{p})\tilde{\Delta}(\boldsymbol{p}')(\boldsymbol{q}\cdot\boldsymbol{q}')^2(\boldsymbol{p}\cdot\boldsymbol{p}')^2
$$
$$
\boldsymbol{k}\cdot(\boldsymbol{p}+\boldsymbol{p}')(\boldsymbol{k}-\boldsymbol{p}-\boldsymbol{p}')\cdot(\boldsymbol{q}+\boldsymbol{q}')
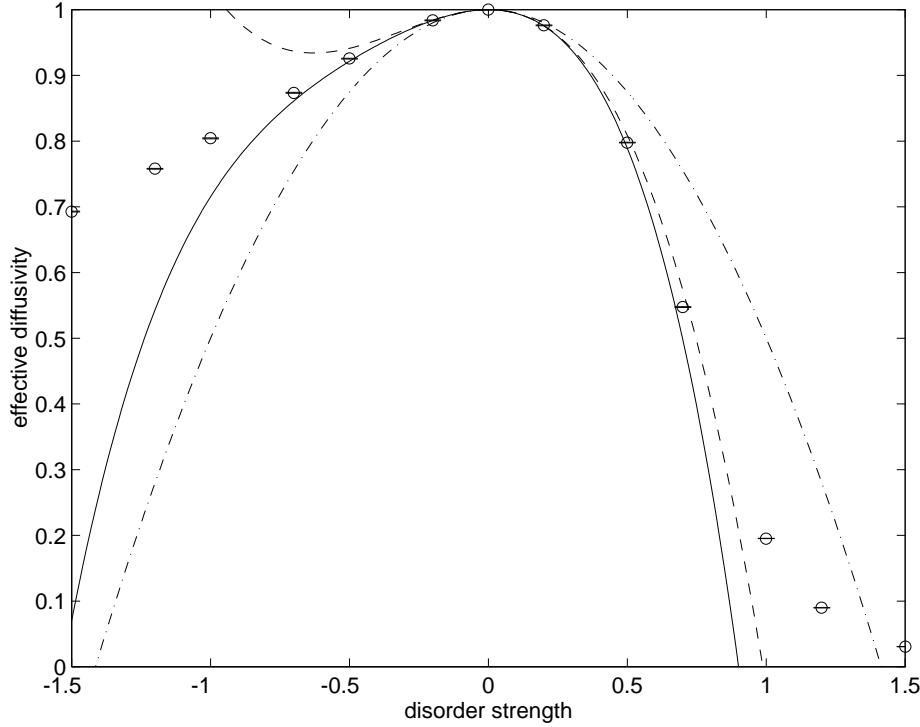$$

Figure 5. κ_e versus λ_0 assuming $\kappa_0 = 1$. The simulation data are shown ($\bigcirc$) to be compared with the prediction of two-loop (chain), three-loop (broken) and four-loop (full) perturbation theory.

$$\frac{(k-p-p'-q-q')\cdot(q+q')(k-p-p')\cdot(p+p')}{(k-p-p')^4(k-p-p'-q-q')^2} \tag{31}$$

$$\overset{(4c)}{\sum}(k) = -\frac{\lambda_0^4}{\kappa_0^3}\int\frac{\mathrm{d}^3q}{(2\pi)^3}\frac{\mathrm{d}^3q'}{(2\pi)^3}\frac{\mathrm{d}^3p}{(2\pi)^3}\frac{\mathrm{d}^3p'}{(2\pi)^3}\tilde{\Delta}(q)\tilde{\Delta}(q')\tilde{\Delta}(p)\tilde{\Delta}(p')\,q\cdot q'\ p\cdot p'\ p'\cdot q\ p\cdot q'$$

$$k\cdot(p+p')(k-p-p')\cdot(q-p')$$

$$\frac{(k-p-q)\cdot(q'-q)(k-p-q')\cdot(p+q')}{(k-p-p')^2(k-p-q)^2(k-p-q')^2} \tag{32}$$

$$\overset{(4d)}{\sum}(k) = -\frac{\lambda_0^4}{\kappa_0^3}\int\frac{\mathrm{d}^3q}{(2\pi)^3}\frac{\mathrm{d}^3q'}{(2\pi)^3}\frac{\mathrm{d}^3p}{(2\pi)^3}\frac{\mathrm{d}^3p'}{(2\pi)^3}\tilde{\Delta}(q)\tilde{\Delta}(q')\tilde{\Delta}(p)\tilde{\Delta}(p')\,q\cdot q'\ p\cdot p'\ p'\cdot q\ p\cdot q'$$

$$k\cdot(p+p')(k-p-p')\cdot(q-p')$$

$$\frac{(k-p-q)\cdot(q'-p)(k-q-q')\cdot(q+q')}{(k-p-p')^2(k-p-q)^2(k-q-q')^2} \tag{33}$$

$$\overset{(4e)}{\sum}(k) = \frac{\lambda_0^4}{\kappa_0^3}\int\frac{\mathrm{d}^3q}{(2\pi)^3}\frac{\mathrm{d}^3q'}{(2\pi)^3}\frac{\mathrm{d}^3p}{(2\pi)^3}\frac{\mathrm{d}^3p'}{(2\pi)^3}\tilde{\Delta}(q)\tilde{\Delta}(q')\tilde{\Delta}(p)\tilde{\Delta}(p')\,q\cdot q'\ p\cdot p'\ p'\cdot q'\ p\cdot q$$

$$k\cdot(p+p')(k-p-p')\cdot(q+q')$$

$$\frac{(k-q-q'-p-p')\cdot(q'+p')(k-q-p)\cdot(q+p)}{(k-p-p')^2(k-q-q'-p-p')^2(k-q-p)^2}. \tag{34}$$

The above expressions can be simplified using the same sort of manipulations as in the three-loop case. The first two are calculated analytically to $O(k^2)$ with the result

$$\sum^{(4,a+b)}(\boldsymbol{k}) = -\frac{1}{8}\frac{\lambda_0^4}{\kappa_0^3}k^2\left[\frac{1}{3}\int\frac{\mathrm{d}^3\boldsymbol{q}}{(2\pi)^3}q^2\tilde{\Delta}(\boldsymbol{q})\right]^4 = -\frac{1}{8}\frac{\lambda_0^4}{\kappa_0^3}k^2. \tag{35}$$

The remaining ones lead, again, to a dominant contribution that can be calculated analytically plus smaller pieces which are evaluated numerically to yield

$$\sum^{(4,c+d+e)}(\boldsymbol{k}) = \frac{\lambda_0^4}{\kappa_0^3}k^2\left(\frac{1}{2} - 0.06\right). \tag{36}$$

The outcome for κ_e to $O(\lambda_0^4)$ is then

$$\kappa_e = \kappa_0\left\{1 - \frac{1}{2}\frac{\lambda_0^2}{\kappa_0^2} - 0.530\,375\frac{\lambda_0^3}{\kappa_0^3} - 0.315\frac{\lambda_0^4}{\kappa_0^4}\right\}. \tag{37}$$

The results for κ_e at two, three and four loops are shown plotted in figure 5 for the range $-1.5 < \lambda_0 < 1.5$ and $\kappa_0 = 1$. Clearly, the four-loop perturbative calculation is successful in surmounting the difficulties of the three-loop case while encoding the deviations from Gaussian behaviour. The latter, are translated into a fast decay of κ_e for positive values of λ_0 whereas it decreases more slowly for the negative values.

3. Numerical simulation of drift and diffusivity

To simulate the evolution of the scalar field $P(\boldsymbol{x}, t)$ we integrate numerically the stochastic equation for the evolution of a particle with path $\boldsymbol{x}(t)$ given by equation (10). The resulting probability distribution for the particle position $\boldsymbol{x}(t)$ is then $P(\boldsymbol{x}, t)$ with the initial condition $P(\boldsymbol{x}, 0) = \delta(\boldsymbol{x})$.

The discrete form of equation (10) suitable for numerical integration is

$$\boldsymbol{x}_{n+1} - \boldsymbol{x}_n = \boldsymbol{u}(\boldsymbol{x}_n)\Delta t + (2\kappa_0\Delta t)^{1/2}\boldsymbol{\xi}_n \tag{38}$$

where $\boldsymbol{\xi}_n$ is a Gaussian random three-vector of zero mean and unit variance for each component. This equation models equation (10) correctly to $O(\Delta t)$ but the details of a third-order Runge–Kutta scheme correct to $O(\Delta t^3)$ are given in [14]. We use this third-order scheme in our numerical simulation.

The realizations of the random field $\phi(\boldsymbol{x})$ are constructed in the usual way [13–15]. We set

$$\phi(\boldsymbol{x}) = \left(\frac{2}{N}\right)^{1/2}\sum_{n=1}^{N}\cos(\boldsymbol{k}_n \cdot \boldsymbol{x} + \epsilon_n) \tag{39}$$

where the vector ϵ_n is distributed uniformly over the unit sphere and the wavevector $\boldsymbol{k}_n$ is distributed according to the distribution

$$P(\boldsymbol{k}) = \frac{1}{(2\pi)^{3/2}}\mathrm{e}^{-k^2/2}. \tag{40}$$

For N sufficiently large the central limit theorem guarantees that $\phi(\boldsymbol{x})$ is Gaussian up to $O(1/N)$ corrections.

The effective diffusivity is computed, for a realization of the velocity field, from the ensemble of paths by

$$\langle \boldsymbol{x}(t) \cdot \boldsymbol{x}(t) \rangle_{\text{paths}} = \lim_{M \to \infty} \frac{1}{M} \sum_{a=1}^{M} \boldsymbol{x}^a(t) \cdot \boldsymbol{x}^a(t)$$

$$= 6\kappa_e t + \mathrm{O}(1) \qquad \text{as } t \to \infty. \tag{41}$$

To measure the effective drift, λ_e, we add a constant drift term to equation (12). In appropriate units, it is given by

$$\boldsymbol{u}' = \lambda_0 \boldsymbol{g} \tag{42}$$

where $\boldsymbol{g}$ is a uniform gradient field. Assuming that the latter lies along the x-axis, for a realization of the velocity field, λ_e is computed according to

$$\langle x(t) \rangle_{\text{paths}} = \lim_{M \to \infty} \frac{1}{M} \sum_{a=1}^{M} x^a(t)$$

$$= \lambda_e g t + \mathrm{O}(1) \qquad \text{as } t \to \infty. \tag{43}$$

In practice, the number of field realizations and M are finite but large enough to give an estimate of κ_e and λ_e with reasonable error. In addition the simulation must be carried to values of t large enough to ensure that measurements are being performed in the asymptotic regime controlled by the long-range or 'renormalized' parameters. This is tested by ensuring that the estimates for κ_e and λ_e are independent of the range of t used to evaluate them, within statistical errors. In our simulation we tracked the trajectories of 400 particles in each of 1280 realizations of the velocity field, each of them containing 128 modes. The simulation was run for a total of 8000 (32 000) time steps of length 0.025 (0.0125) for the smaller (larger) absolute values of the bare coupling λ_0. For larger values of λ_0 and because of time limitations the number of paths followed was reduced to a minimum of a hundred.

The results from the perturbation theory calculation of κ_e against results from the simulation are shown in figure 5 for the range $-1.5 < \lambda_0 < 1.5$ and assuming $\kappa_0 = 1$. The simulation confirms the pronounced asymmetry of κ_e as a function of λ_0, exhibiting a fast (slow) decay for positive (negative) values of λ_0. The four-loop order results compare well with the simulation outcome in the range $-0.7 < \lambda_0 < 0.7$. As expected, the four-loop perturbative calculation encodes the relevant qualitative features of the flow and is effective in the region of small disorder as opposed to the two-loop and three-loop case.

In table 1 we show the measurements of both κ_e and λ_e over a range of values of the disorder parameter (again, we take $\kappa_0 = 1$). The results clearly show that the equality of the two renormalized factors is well maintained throughout with only slight discrepancies some cases due to systematic errors. For the higher values of the disorder parameter another possible source of error is that the value of the drift parameter has become so large that $\mathrm{O}(g^2)$ effects are influencing the values of the measured quantities. Nevertheless, we are confident that the simulation supports the conclusion that in gradient flow, irrespective of the precise nature of the statistics of the velocity field, the drift and diffusivity parameters are renormalized in the same way if we start from a situation where the corresponding microscopic quantities are proportional. This result confirms the theoretical prediction previously obtained in [10] using a theoretical approach developed for the continuum from a method due to Derrida [1, 16, 17].

Table 1. Measurements of κ_e and λ_e for various values of the disorder parameter λ_0.

λ_0	g	κ_e	(λ_e/λ_0)
−2.0	0.05	0.600 93(52)	0.6014(7)
−1.5	0.05	0.692 76(60)	0.6946(9)
−1.2	0.05	0.757 97(66)	0.7583(12)
−1.0	0.05	0.804 12(69)	0.8032(15)
−0.7	0.05	0.873 60(75)	0.8753(31)
−0.5	0.05	0.925 60(56)	0.9213(32)
−0.2	0.125	0.983 86(59)	0.9803(33)
0.2	0.125	0.976 32(59)	0.9790(33)
0.5	0.05	0.797 88(49)	0.7983(30)
0.7	0.05	0.547 44(52)	0.5458(25)
1.0	0.05	0.195 37(25)	0.1939(8)
1.2	0.05	0.089 79(15)	0.0895(5)
1.5	0.05	0.030 59(7)	0.0296(3)
2.0	0.05	0.007 90(3)	0.0070(1)

4. Conclusions

In this paper we have studied the motion of a neutral molecule in a random gradient flow. The suggested physical mechanism giving rise to the local drift involves the interaction of the local electric field (presumed to have Gaussian statistics) with the field-induced dipole moment of the molecule. The resulting drift field therefore does *not* have Gaussian statistics. That such a physically plausible model can give rise, in a natural way, to a drift field with non-Gaussian statistics, is itself interesting.

The increased complexity of the model is no barrier to the formulation of a perturbative calculation of its Green functions and effective parameters. The non-Gaussian character of the drift field statistics shows up first at three-loop order. It results in a contribution to the effective diffusivity that is not symmetric under a change of sign of the coupling. This asymmetry is very clear in both the perturbation theory and numerical results exhibited in figure 5. The same figure also exhibits the results of the numerical simulation. It shows that the inclusion of the four-loop terms allows the perturbation series to give a reasonably good account of the effective diffusivity for the coupling parameter in the range $-0.7 < \lambda_0 < 0.7$.

The complexity of the non-Gaussian model, however, has so far prevented, a satisfactory formulation of the kinds of self-consistent perturbative calculation or renormalization group calculation that were rather successful for the Gaussian model [2–6]. In both cases the problem centres round the new types of vertices, not present in the original perturbation theory scheme, that are *induced* by the loop contributions of perturbation theory. The formulation of effective calculational schemes of this kind remains an aim of great interest since, as is clear from figure 5, low-order perturbation theory is inadequate for situations of large disorder. Further investigations are in progress.

In addition to the effective diffusivity the effective drift parameter, which controls the response of the molecules to an externally applied constant gradient field, is also a significant physical quantity. The success of the renormalization group calculation in the Gaussian model was in part due to the fact that it respected the Einstein relation, namely that the effective diffusivity and drift parameter are renormalized by the same factor from their molecular values. The Einstein relation was also demonstrated in low-order perturbation theory. In fact the Einstein relation was later shown to hold quite generally, independently of the statistical properties of the random medium, provided the molecular drift and diffusivity

tensors were proportional to one another [10]: the Gaussian character of the model is not relevant. It is therefore important that we have been able to give numerical confirmation (see table 1) of the validity of the Einstein relation between effective drift and diffusivity in the non-Gaussian model investigated in this paper.

The introduction of directional effects into the drift and diffusivity as well as the statistics of the drift field, are further problems of great interest but considerably increased complexity.

Acknowledgments

References

[1] Bouchaud J-P and Georges A 1990 *Phys. Rep.* **195**
[2] Kravtsov V E, Lerner I V and Yudson V I 1986 *Zh. Eksp. Teor. Fiz.* **91** 569 (Engl. transl. 1986 *Sov. Phys.–JETP* **64** 336)
[3] Kravtsov V E, Lerner I V and Yudson V I 1986 *J. Phys. A: Math. Gen.* **119** 203
[4] Deem M W and Chandler D 1994 *J. Stat. Phys.* **76** 911
[5] Dean D S 1993 Stochastic dynamics *PhD Thesis* University of Cambridge
[6] Dean D S, Drummond I T and Horgan R R 1994 *J. Phys. A: Math. Gen.* **27** 5135
[7] Dean D S, Drummond I T and Horgan R R 1995 *J. Phys. A: Math. Gen.* **28** 1235
[8] Dean D S, Drummond I T and Horgan R R 1995 *J. Phys. A: Math. Gen.* **28** 6013–25
[9] Dean D S, Drummond I T and Horgan R R 1996 *J. Phys. A: Math. Gen.* **29** 7867–79
[10] Dean D S, Drummond I T and Horgan R R 1996 *J. Phys. A: Math. Gen.* **30** 385–96
[11] Goncalves Sousa J A, Portsmouth R L, Alexander P and Gladden L F 1995 *J. Phys. Chem.* **99** 3317–25
[12] Phythian R and Curtis W D 1978 *J. Fluid Mech.* **89** 241
[13] Kraichnan R H 1976 *J. Fluid Mech.* **77** 753
[14] Drummond I T, Duane S and Horgan R R 1984 *J. Fluid Mech.* **138** 75
[15] Drummond I T and Horgan R R 1987 *J. Phys. A: Math. Gen.* **20** 4661
[16] Derrida B 1983 *J. Stat. Phys.* **31** 433
[17] Bouchaud J-P and Le Doussal P 1985 *J. Stat. Phys.* **41** 225